SEE COMMENTARY

UCP1 deficiency causes brown fat respiratory chain depletion and sensitizes mitochondria to calcium overload-induced dysfunction

Lawrence Kazak[a,b,1], Edward T. Chouchani[a,b,1], Irina G. Stavrovskaya[c], Gina Z. Lu[a], Mark P. Jedrychowski[b], Daniel F. Egan[a,b], Manju Kumari[d,e], Xingxing Kong[d,e], Brian K. Erickson[b], John Szpyt[b], Evan D. Rosen[d,e], Michael P. Murphy[f], Bruce S. Kristal[c,g,h], Steven P. Gygi[b], and Bruce M. Spiegelman[a,b,2]

[a]Department of Cancer Biology, Dana-Farber Cancer Institute, Boston, MA 02115; [b]Department of Cell Biology, Harvard Medical School, Boston, MA 02115; [c]Department of Neurosurgery, Brigham and Women's Hospital and Harvard Medical School, Boston, MA 02215; [d]Division of Endocrinology, Beth Israel Deaconess Medical Center, Boston, MA 02215; [e]Department of Genetics, Harvard Medical School, Boston, MA 02215; [f]MRC Mitochondrial Biology Unit, University of Cambridge, Cambridge CB2 0XY, United Kingdom; [g]Division of Sleep and Circadian Disorders, Department of Medicine, Brigham and Women's Hospital, Boston, MA 02215; and [h]Division of Sleep Medicine, Department of Medicine, Harvard Medical School, Boston, MA 02115

Contributed by Bruce M. Spiegelman, May 22, 2017 (sent for review April 3, 2017; reviewed by Martin Jastroch and Steven A. Kliewer)

Brown adipose tissue (BAT) mitochondria exhibit high oxidative capacity and abundant expression of both electron transport chain components and uncoupling protein 1 (UCP1). UCP1 dissipates the mitochondrial proton motive force (Δp) generated by the respiratory chain and increases thermogenesis. Here we find that in mice genetically lacking UCP1, cold-induced activation of metabolism triggers innate immune signaling and markers of cell death in BAT. Moreover, global proteomic analysis reveals that this cascade induced by UCP1 deletion is associated with a dramatic reduction in electron transport chain abundance. UCP1-deficient BAT mitochondria exhibit reduced mitochondrial calcium buffering capacity and are highly sensitive to mitochondrial permeability transition induced by reactive oxygen species (ROS) and calcium overload. This dysfunction depends on ROS production by reverse electron transport through mitochondrial complex I, and can be rescued by inhibition of electron transfer through complex I or pharmacologic depletion of ROS levels. Our findings indicate that the interscapular BAT of *Ucp1* knockout mice exhibits mitochondrial disruptions that extend well beyond the deletion of UCP1 itself. This finding should be carefully considered when using this mouse model to examine the role of UCP1 in physiology.

brown fat | mitochondria | ROS | UCP1 | electron transport chain

Uncoupling protein 1 (UCP1) plays a role in acute adaptive thermogenesis in interscapular brown adipose tissue (BAT). UCP1 dissipates the mitochondrial protonmotive force (Δp) generated by the electron transport chain (ETC) and is important for thermal homeostasis in rodents and human infants (1, 2). *Ucp1* orthologs are not limited to mammals, but are also expressed in ectothermic vertebrates (3) and protoendothermic mammals (4), suggesting that UCP1 may have an important role in biology beyond thermal control. For example, it is becoming increasingly evident that in specific respiratory states, UCP1 can reduce reactive oxygen species (ROS) levels in vitro (4–9). The mitochondrial ETC is a major source of ROS production in the cell, and ROS play important roles in physiology and pathophysiology (10–12). Reverse electron transport (RET) through mitochondrial complex I is a key mechanism by which ROS are generated in vivo (11, 13). Interestingly, RET relies critically on high Δp, whereas dissipation of Δp by UCP1 can lower ROS levels in isolated mitochondria (5–7).

Thermogenic respiration in BAT is triggered by external stimuli that activate adrenergic signaling (14). Most notably, environmental cold induces the capacity for adrenergic-mediated BAT respiration in wild type (WT) animals, but only minimally in UCP1-KO animals (15, 16). It is understood that the respiratory response of BAT under these conditions is indicative of UCP1-mediated respiration; however, the rate of maximal chemically uncoupled oxygen consumption, an UCP1-independent parameter, is also lower in UCP1-KO adipocytes compared with WT (15, 16). Moreover, the basal respiratory rate of UCP1-KO BAT mitochondria is reduced after cold exposure, whereas it is increased in WT BAT mitochondria (7). These data strongly suggest broader functional changes to brown adipocyte mitochondrial function on increased adrenergic tone following *Ucp1* deletion.

Here we demonstrate that extensive down-regulation of ETC abundance and concomitant triggering of host defense signaling occurs in BAT of UCP1-KO mice following cold acclimation. Remarkably, UCP1-KO BAT mitochondria are highly sensitive to calcium overload-induced mitochondrial dysfunction, which can be inhibited by reducing ROS levels. These findings suggest a critical physiological role of UCP1 in maintaining a mitochondrial environment that can mitigate ROS-dependent dysfunction in vivo. In addition, these data demonstrate that the absence of UCP1 in BAT results in widespread mitochondrial proteomic alterations that should be considered when using this mouse model to examine the role of UCP1 in physiology.

Results

Aberrant Cristae Morphology and Reduced ETC Abundance in UCP1-KO BAT. Environmental cold increases state 4 respiration in mitochondria isolated from BAT of WT mice, and substantially

Significance

We describe a physiological role for uncoupling protein 1 (UCP1) in the regulation of reactive oxygen species. Notably, the molecular differences between brown fat mitochondria from wild-type and UCP1 knockout (UCP1-KO) mice extend substantially beyond the deletion of UCP1 itself. Thus, caution must be taken when attributing a brown fat phenotype solely to UCP1 deletion when these animals are used. Given the wide utilization of the UCP1-KO mouse model, these data are of critical importance for the scientific communities studying obesity, thermogenesis and energy metabolism, and mitochondrial biology.

Author contributions: L.K. designed research; L.K., E.T.C., I.G.S., G.Z.L., M.P.J., D.F.E., M.K., X.K., B.K.E., and J.S. performed research; E.D.R., M.P.M., B.S.K., and S.P.G. contributed new reagents/analytic tools; L.K. analyzed data; and L.K., E.T.C., M.P.M., and B.M.S. wrote the paper.

Reviewers: M.J., Institute for Diabetes and Obesity, Helmholtz Zentrum München, German Research Center for Environmental Health; and S.A.K., University of Texas Southwestern Medical Center at Dallas.

The authors declare no conflict of interest.

Freely available online through the PNAS open access option.

See Commentary on page 7744.

[1]L.K. and E.T.C. contributed equally to this work.

[2]To whom correspondence should be addressed: Email: Bruce_Spiegelman@dfci.harvard.edu.

This article contains supporting information online at www.pnas.org/lookup/suppl/doi:10.1073/pnas.1705406114/-/DCSupplemental.

reduces it in BAT mitochondria from UCP1-KO mice (7, 17). These previous studies have suggested that ETC expression is impaired after adrenergic stimulation of BAT in the absence of UCP1. To investigate the role of UCP1 on BAT mitochondria on adrenergic stimulation, we gradually acclimated WT and UCP1-KO mice to cold (4 °C) and assessed gross mitochondrial morphology by electron microscopy. Remarkably, this analysis revealed highly disorganized and in some cases absent cristae from UCP1-KO organelles relative to WT organelles (Fig. 1*A*). This aberrant morphology prompted us to examine the molecular components of BAT mitochondria that might be affected by the absence of UCP1 under conditions of adrenergic stimulation.

To determine the mitochondrial molecular response in WT and UCP1-KO BAT after cold exposure, we began by measuring the mRNA abundance of nuclear-encoded subunits of the oxidative phosphorylation complexes. A subset of transcripts was significantly reduced in response to environmental cold in a UCP1-dependent manner; however, the extent of reduction was modest (Fig. S1). In contrast, no differences in mRNA abundance in BAT were detected between UCP1-KO and WT mice under thermoneutral (30 °C) housing (Fig. S1). This was a general feature for nuclear-encoded genes of all the oxidative phosphorylation complexes.

The mild diminution of nuclear-encoded oxidative phosphorylation complexes (Fig. S1) prompted us to investigate their abundance at the protein level. To do so, we performed global quantitative proteomics in BAT of cold-acclimated WT and UCP1-KO mice using isobaric tagging (18), which provided quantitation of 6,354 proteins (Dataset S1). Unsupervised *k*-means clustering of the proteomic data revealed a total of six clusters (Datasets S2–S7), two of which (clusters 4 and 5) were robustly distinct between WT and UCP1-KO BAT (Fig. 1*B*). The top KEGG pathway of cluster 5 was designated as "oxidative phosphorylation," consisting primarily of ETC proteins (Dataset S6). The protein abundance in this cluster was substantially reduced in UCP1-KO relative to WT BAT (Fig. 1*B* and Dataset S1). The percentage reduction (>80%) at the protein level (Dataset S1) was discordant with the relatively mild decrease in corresponding transcript abundance (Fig. S1). Most subunits of complexes I and IV were down-regulated (up to 95%) compared with BAT from WT mice (Dataset S1).

We next examined protein abundance by Western blot analysis in a separate cohort of mice housed at 4 °C or 30 °C. As in the MS analysis, ETC subunits were considerably reduced in UCP1-KO BAT tissue lysates, primarily on 4 °C exposure. Interestingly, these reductions in ETC abundance were not nearly as drastic in adult animals housed at 30 °C (Fig. 1*C*). Notably, there were no differences in ETC protein expression in young (postnatal day 4) pups (Fig. 1*D*), suggesting that the impaired ETC expression seen at older ages was primarily a response to environmental cold specifically and not due to aberrant BAT development. We next examined the expression of these proteins after mitochondrial purification. Strikingly, the depletion in ETC proteins was also

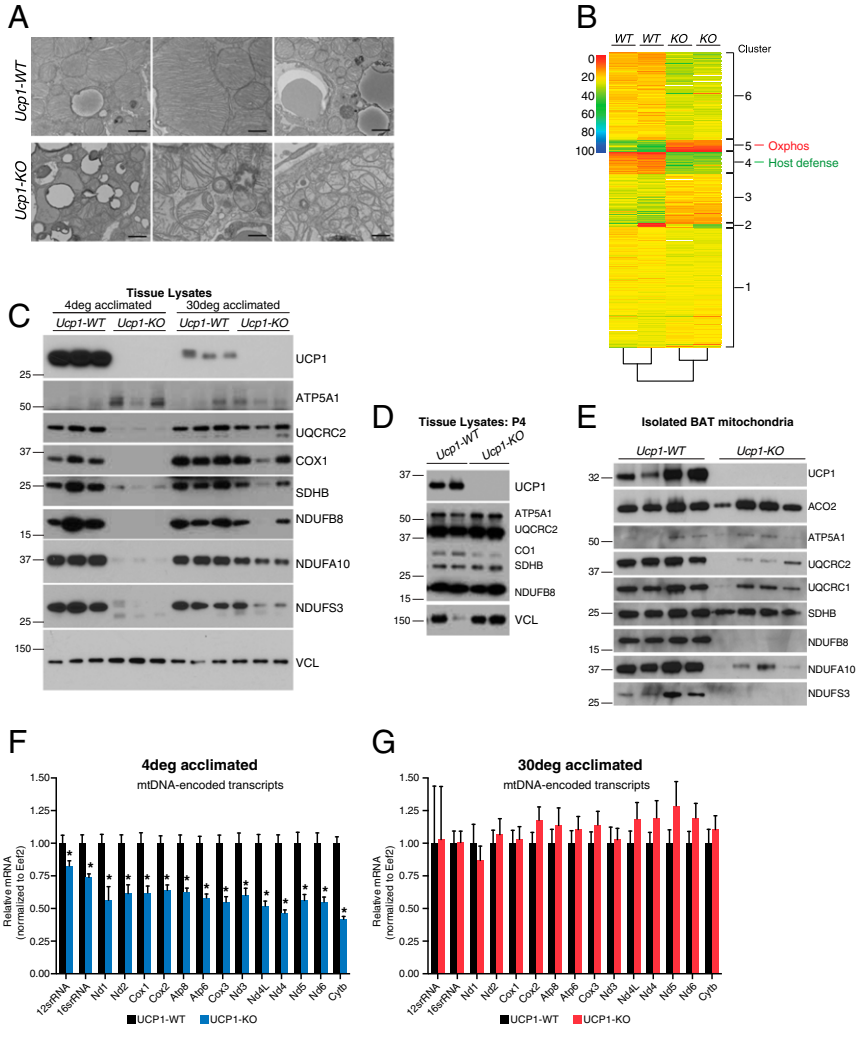

Fig. 1. Mitochondrial morphology and protein expression in BAT of WT and UCP1-KO animals. (*A*) Electron microscopy images of WT and UCP1-KO BAT following 3 wk cold exposure of mice. (*B*) Heatmap of BAT proteomics data (from Dataset S1). (*C*) Western blot of mitochondrial proteins from WT and UCP1-KO BAT after housing adult animals at 4 °C or 30 °C. (*D*) Western blot of mitochondrial proteins from WT and UCP1-KO BAT from postnatal day 4 pups. (*E*) Western blot of mitochondrial proteins from WT and UCP1-KO BAT mitochondria. (*F*) qRT-PCR of mtDNA-encoded transcripts in BAT from WT and UCP1-KO mice housed at 4 °C; $n = 5$ mice per genotype. (*G*) qRT-PCR of mtDNA-encoded transcripts in BAT from WT and UCP1-KO mice housed at 30 °C; $n = 5$ mice per genotype. Data are presented as mean ± SEM. $^{*}P < 0.05$; $^{***}P < 0.01$.

observed in isolated organelles (Fig. 1*E*), demonstrating that the decrease in protein expression was not due solely to a reduction in mitochondrial mass. Interestingly, the succinate dehydrogenase complex iron sulfur subunit B of complex II showed minimal differences when we controlled for total mitochondrial abundance (Fig. 1*E*). Because succinate dehydrogenase is the only ETC complex that is entirely nuclear-encoded, these data suggest a specific effect on ETC complexes containing gene products encoded by mitochondrial DNA (mtDNA) owing to the absence of UCP1.

Environmental Cold Triggers Loss of mtDNA Transcripts in UCP1-KO BAT. mtDNA is physically associated with the mitochondrial inner membrane in DNA-protein complexes known as nucleoids (19, 20), and a disturbance in this association is known to disrupt mtDNA-encoded gene expression. Thus, given the aberrant cristae morphology of UCP1-KO BAT mitochondria after exposure to 4 °C (Fig. 1*A*), along with the specific reduction in ETC complexes containing mtDNA-encoded gene products (Fig. 1*E*), we examined the expression level of mtDNA-encoded transcripts. Strikingly, all mtDNA-encoded transcripts, as well as the two mitochondrial rRNA transcripts, were significantly reduced in BAT of UCP1-KO mice after exposure to environmental cold (Fig. 1*F*). In contrast, when mice were housed at 30 °C, no change in mRNA abundance between the genotypes was detected (Fig. 1*G*).

Environmental Cold Triggers Host Defenses in UCP1-KO BAT. In contrast to the large reduction in ETC subunits, quantitative proteomic profiling of BAT from WT and UCP1-KO mice revealed an additional cluster (cluster 4), highlighting increased levels of proteins involved in host defense (Fig. 1*B* and Dataset S5). Included in this cluster was an increase in IFN-stimulated genes (ISGs) and antiviral factors encoding DNA and RNA sensors, such as *Ifi204*, *Ifi205*, *Ifih1*, and *Ddx58*, as well as the transcription factors *Stat1*, *Stat2*, and *Irf3* (Dataset S1).

Because these factors function to reinforce the innate and adaptive immune response (21), we next examined the control of ISG expression by ambient temperature. ISGs (*Ifit1*, *Ifit2*, *Ifit3*, *Oas3*, and *RNase L*) were significantly elevated at the mRNA level in BAT of 4 °C-exposed UCP1-KO mice relative to WT controls (Fig. 2*A*); however, these changes were largely abolished when mice were housed at 30 °C (Fig. 2*B*). We found elevated

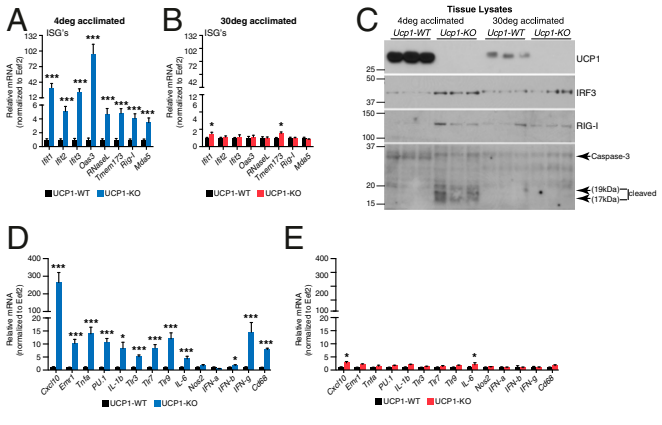

Fig. 2. Expression of genes and proteins involved in host defense in BAT of WT and UCP1-KO animals. (*A*) qRT-PCR of ISG expression in BAT from WT and UCP1-KO mice housed at 4 °C; $n = 5$ mice per genotype. (*B*) qRT-PCR of ISG expression in BAT from WT and UCP1-KO mice housed at 30 °C; $n = 5$ mice per genotype. (*C*) Western blot of antiviral and cell death proteins in BAT from WT and UCP1-KO animals after exposure to 4 °C or 30 °C. (*D*) qRT-PCR of inflammatory gene expression in BAT from WT and UCP1-KO mice housed at 4 °C; $n = 5$ mice per genotype. (*E*) qRT-PCR of inflammatory gene expression in BAT from WT and UCP1-KO mice housed at 30 °C; $n = 5$ mice per genotype. Data are presented as mean ± SEM. $^*P < 0.05$; $^{***}P < 0.01$.

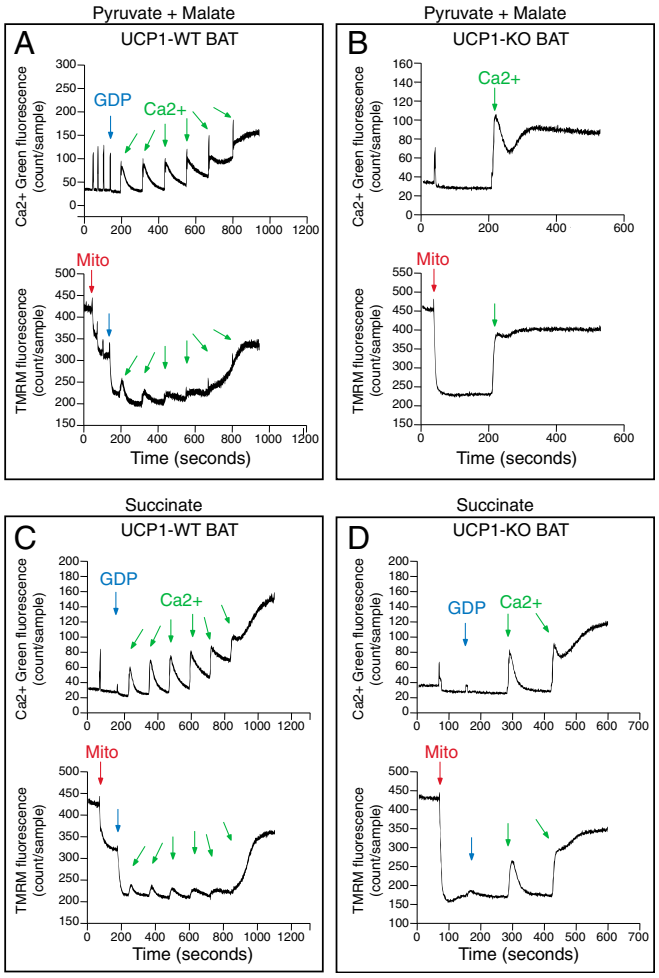

Fig. 3. Simultaneous monitoring of mitochondrial calcium buffering capacity and membrane potential. (*A*) Calcium (Ca^{2+}) and TMRM monitoring of WT BAT mitochondria respiring on pyruvate/malate. (*B*) Ca^{2+} and TMRM monitoring of UCP1-KO BAT mitochondria respiring on pyruvate/malate without GDP. (*C*) Ca^{2+} and TMRM monitoring of WT BAT mitochondria respiring on succinate. (*D*) Ca^{2+} and TMRM monitoring of UCP1-KO BAT mitochondria respiring on succinate. Images shown are representative of at least three independent mitochondrial preparations for each substrate used. Arrows indicate the addition of mitochondria (red), GDP (blue), and calcium (green).

levels of the nucleic acid-sensing factor RIG-I and the antiviral transcription factor IRF3 in UCP1-KO mice compared with WT mice housed at 4 °C, whereas housing at 30 °C abrogated the difference between the genotypes (Fig. 2*C* and Dataset S1). IRF3 represses thermogenic gene expression (22). Interestingly, the thermogenic transcription factor Prdm16 suppresses ISG expression (23). Our data extend these findings by demonstrating that the capacity for thermogenic respiration itself may regulate ISG abundance. This result highlights the interconnected relationship between the thermogenic and host defense transcriptional machinery and the effectors of thermogenic respiration. Furthermore, in line with the higher levels of ISG expression, cleaved caspase-3 levels were elevated in UCP1-KO BAT after exposure to 4 °C, but not when mice were housed at 30 °C (Fig. 2*C*). Caspase activation dampens the immune response and triggers mitochondrial-mediated programmed cell death (24).

To explore whether activation of the immune response is regulated by ambient temperature, we examined a panel of inflammatory genes from BAT of WT and UCP1-KO mice housed under cold or thermoneutral conditions by quantitative RT-PCR (qRT-PCR). We detected robust elevation of inflammatory

genes, including those associated with innate immunity, IFN-γ signaling, and macrophage infiltration, in the UCP1-KO mice housed at 4 °C (Fig. 2*D*). Remarkably, housing mice at 30 °C largely abolished this inflammatory response (Fig. 2*E*). Taken together, the foregoing data demonstrate that environmental cold triggers mitochondrial dysfunction and antiviral signaling in UCP1-deficient BAT. The data suggest that on cold stimulation, absence of *Ucp1* results in aberrant BAT mitochondrial function, leading to mitochondrial-mediated triggering of immune activation.

Calcium Overload Induces Mitochondrial Dysfunction in UCP1-KO BAT. Cold stimulation drives the activation of innate immune pathways linked to cell death. Because mitochondrial permeability transition is a well-established regulator of this process (25), we examined whether UCP1-KO BAT mitochondria are inherently sensitive to permeability transition by challenging organelles with calcium. We simultaneously measured the mitochondrial membrane potential (Δψ) and calcium-buffering capacity in BAT mitochondria isolated from WT and UCP1-KO mice. WT BAT mitochondria respiring on pyruvate and malate exhibited a modest Δψ, indicated by the downward inflection in the tetramethylrhodamine, methyl ester (TMRM) signal on addition of the organelles. This was increased after GDP administration, demonstrating inhibition of UCP1-dependent leak (Fig. 3*A*, *Bottom*).

We next treated mitochondria with sequential additions of calcium (26). Each calcium addition could be observed as an increase in Calcium Green fluorescence in the buffer, whereas uptake into the organelles was reflected in a reduction in buffer calcium (Fig. 3*A*, *Top*). Mitochondrial membrane depolarization occurred concomitantly with each addition of calcium (60 nmol calcium/mg mitochondrial protein), followed by rapid repolarization (Fig. 3*A*, *Bottom*). Here 300 nmol calcium/mg mitochondrial protein could be buffered by WT BAT mitochondria, whereas calcium release occurred thereafter (Fig. 3*A*, *Top*). Depolarization of Δψ occurred concomitantly with calcium release. UCP1-KO BAT mitochondria exhibited a similar baseline Δψ as GDP-treated WT mitochondria (Fig. 3*B*, *Bottom*); however, the addition of calcium to UCP1-KO organelles resulted in a significant depolarization of Δψ (Fig. 3*B*, *Bottom*). Furthermore, a single calcium addition (60 nmol calcium/mg mitochondrial protein) was poorly buffered by UCP1-KO mitochondria and was sufficient to result in concomitant calcium release and depolarization (Fig. 3*B*). These data indicate that UCP1-KO BAT mitochondria have substantially reduced calcium-buffering capacity compared with WT organelles. Permeability transition can be inhibited by the drug cyclosporin A (27), and we detected a modest protective effect of this compound on UCP1-KO mitochondrial calcium buffering capacity (Fig. S2), which is consistent with previous findings (28). Taken together, these data demonstrate that UCP1-KO BAT mitochondria are sensitized to calcium overload-induced mitochondrial dysfunction, a component of which is partly inhibited by cyclosporin A.

We next examined calcium kinetics and Δψ during succinate-dependent respiration. WT BAT mitochondria respiring on succinate responded similarly as when pyruvate and malate were used to drive respiration through complex I. A total of 300 nmol calcium/mg mitochondrial protein was efficiently buffered by WT BAT mitochondria (Fig. 3*C*). In contrast, UCP1-deficient BAT mitochondria could buffer only 60 nmol calcium/mg mitochondrial protein (Fig. 3*D*). Therefore, UCP1 deficiency results in a profound sensitization to calcium-overload induced dysfunction in mitochondria respiring on succinate.

ROS Triggers Calcium Overload-Induced Mitochondrial Dysfunction in UCP1-KO BAT. Succinate oxidation can drive RET, and so can be used to investigate complex I-dependent ROS (11, 29–31). Complex I is the dominant site of superoxide production when mitochondria respire on succinate (29, 32). Under conditions of high membrane potential, succinate reduces ubiquinone (Q) to ubiquinol (QH_2), resulting in a reverse electron flow through

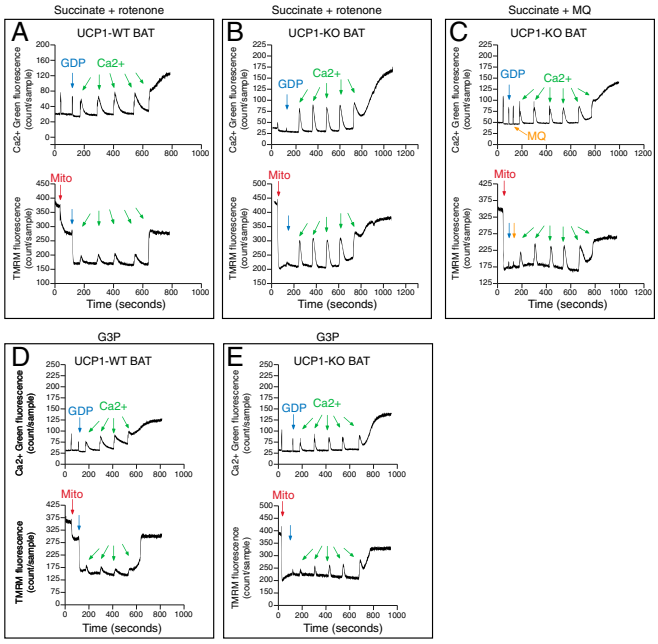

Fig. 4. The role of ROS in mitochondrial calcium buffering capacity and membrane potential. (*A*) Ca^{2+} and TMRM monitoring of WT BAT mitochondria respiring on succinate/rotenone. (*B*) Ca^{2+} and TMRM monitoring of UCP1-KO BAT mitochondria respiring on succinate/rotenone. (*C*) Ca^{2+} and TMRM monitoring of UCP-KO BAT mitochondria respiring on succinate in the presence of 100 nM MitoQ. (*D*) Ca^{2+} and TMRM monitoring of WT BAT mitochondria respiring on G3P. (*E*) Ca^{2+} and TMRM monitoring of UCP1-KO BAT mitochondria respiring on G3P. Images shown are representative of at least three independent mitochondrial preparations for each substrate used. Arrows indicate the addition of mitochondria (red), GDP (blue), calcium (green), or MitoQ (yellow).

complex I (11, 30). Under these circumstances, single electron reduction of oxygen can generate substantial levels of superoxide, and this has been proposed to occur at the FMN site of complex I (32, 33) or, alternatively, the IQ site (30). The complex I Q site inhibitor rotenone inhibits RET-driven superoxide production during succinate oxidation (29, 34–37). Critically, mitochondrial ROS has been demonstrated to potentiate calcium-dependent permeability transition (25, 38). Moreover, succinate has been shown to generate significant amounts of ROS in BAT, which is exacerbated in the absence of UCP1 (7, 8). Thus, we evaluated the contribution of ROS to the observed calcium sensitivity of UCP1-KO BAT mitochondria. Inhibition of RET with rotenone had no effect on the calcium-buffering properties of WT BAT mitochondria (Fig. 4*A*); however, inhibition of RET rescued the calcium-induced dysfunction of UCP1-KO BAT mitochondria (Fig. 4*B*, *Top*). Although each addition of calcium still caused a large transient depolarization and slow repolarization (Fig. 4*B*, *Bottom*), the amount of calcium required to drive complete membrane depolarization was completely normalized. Therefore, inhibiting RET through complex I essentially restored the calcium retention time and buffering capacity of UCP1-KO BAT mitochondria to WT levels.

To further explore whether elevated ROS levels are responsible for the calcium-induced dysfunction, we treated UCP1-KO BAT mitochondria with the mitochondria-targeted antioxidant MitoQ (39) just before the calcium challenge. Like rotenone, MitoQ rescued the calcium buffering capacity of UCP1-KO organelles (Fig. 4*C*). The large depolarization and slow repolarization of Δψ (Fig. 4*C*, *Bottom*) are consistent with abrogated ETC expression. Collectively, these results suggest that UCP1-KO BAT mitochondria are extraordinarily sensitive to ROS-dependent permeability transition. Interestingly, we did not observe large differences between genotypes when G3P was used as a respiratory substrate (Fig. 4 *D* and *E*).

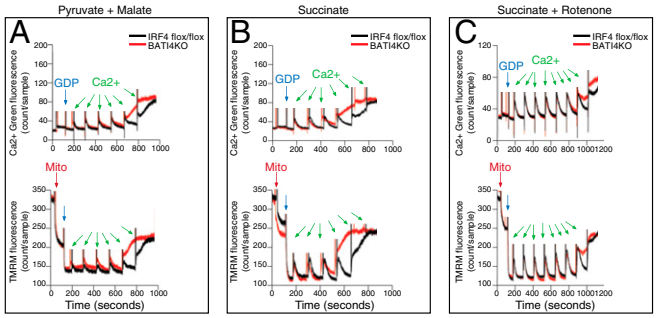

Fig. 5. The role of ROS in mitochondrial calcium buffering capacity and membrane potential in BAT of BATI4KO mice. (*A*) Ca^{2+} and TMRM monitoring of WT and BATI4KO BAT mitochondria respiring on pyruvate/malate. (*B*) Ca^{2+} and TMRM monitoring of WT and BATI4KO BAT mitochondria respiring on succinate. (*C*) Ca^{2+} and TMRM monitoring of WT and BATI4KO BAT mitochondria respiring on succinate/rotenone.

Finally, to examine whether the calcium-induced sensitivity of UCP1-KO BAT mitochondria is a feature of these organelles specifically or a feature of UCP1 deficiency generally, we examined the calcium-buffering capacity and $\Delta\psi$ in mitochondria from BAT-specific IRF4 KO mice (BATI4KO) that exhibit reduced UCP1 levels in BAT (40). Similar to what we observed in UCP1-KO BAT mitochondria, organelles from BATI4KO mice demonstrated increased sensitivity to calcium overload-induced permeability transition when respiring on pyruvate/malate (Fig. 5*A*) or succinate (Fig. 5*B*). Although the sensitivity to calcium overload of BAT14KO mitochondria was not as striking as that of UCP1-KO BAT mitochondria, it still could be partially rescued by rotenone treatment (Fig. 5*C*). Because BAT mitochondria from BATI4KO mice contain lower levels of UCP1 and complex I protein (40), these results suggest that calcium overload-induced mitochondrial dysfunction may be a general phenomenon of BAT mitochondria under conditions with reduced UCP1 expression.

Discussion

UCP1 is a key feature of thermogenic fat cells, both brown and beige. We have demonstrated here that on cold exposure, interscapular BAT of UCP1-KO mice exhibits global mitochondrial disruptions that extend well beyond the deletion of UCP1 itself. Our data reveal physiological interactions between UCP1 and ROS. The role of UCP1 itself in the regulation of ROS production is incompletely understood. Evidence in support of a robust role for UCP1-mediated uncoupling in the regulation of ROS production in vitro has been provided (6, 7, 41), as have findings suggesting a limited role for UCP1 activity in controlling ROS in vitro (8, 42–44). Importantly, UCP1 appears to play a role in regulating BAT redox tone in vivo (9), and acute adrenergic stimulation in vivo drives ROS production to support UCP1-dependent thermogenesis (10).

Our findings demonstrate that UCP1-deficient BAT mitochondria are poorly equipped to buffer calcium in a ROS-dependent manner. Most importantly, we have shown that the acquired molecular and functional differences between BAT mitochondria from WT and UCP1-KO mice are more widespread than the deletion of UCP1 itself. Considering the striking alterations to the BAT mitochondrial proteome (i.e., substantial reduction of ETC abundance) in UCP1-KO mice, caution must be observed when attributing a BAT phenotype solely to UCP1 deletion in these animals. In addition, reduced ETC expression may be commonly associated with decreased UCP1 levels more generally, which should be kept in mind when studying genetic models with reduced BAT UCP1 expression. Notably, our findings reported here suggest that the reduced capacity of UCP1-KO BAT to activate oxidative metabolism after adrenergic administration (cold or chemical) is due at least in part to reduced expression of the ETC, and not solely to lack of UCP1-mediated uncoupling.

Examination of calcium sensitivity of BAT mitochondria with and without UCP1 adds further evidence supporting the relevance of the mechanisms of ROS production in BAT. Previous studies comparing ROS production between WT and UCP1-KO BAT mitochondria when using G3P as a respiratory substrate have indicated either comparable (8) or enhanced (6, 7) levels. Importantly, G3P-mediated mitochondrial energization can drive ROS production by RET or from mitochondrial G3P dehydrogenase (GPD2) itself (7, 30). Moreover, GPD2 appears to have the capacity to produce ROS in the mitochondrial intermembrane space (30, 41, 45), as opposed to complex I, which produces superoxide in the mitochondrial matrix (12). This compartmentalization of ROS production is a plausible explanation for the sensitivity of UCP1-KO mitochondria to succinate-mediated ROS production, which drives superoxide production principally through complex I (12). Because G3P-mediated ROS production can drive ROS independently of complex 1 (i.e., at GPD2 itself) (7, 30, 41), our data suggest that complex I-mediated ROS production by RET is a major contributor to mitochondrial dysfunction in UCP1-KO BAT. This interpretation is in line with the recognized importance of ROS originating in the mitochondrial matrix supporting permeability transition (46, 47). Interestingly, GPD2 abundance was unaltered in UCP1-KO BAT (Dataset S1), suggesting that in the absence of UCP1, G3P-mediated electron flux to coenzyme Q is maintained. Previous investigations have noted quantitatively different effects of G3P-driven ROS production in BAT mitochondria between WT and UCP1-KO animals (6–8). Considering our findings, these discrepancies may be predictive of differential mitochondrial adaptation in different UCP1-KO mice colonies to mitigate ROS sensitivity owing to a genetic absence of UCP1. Such differences might be expected to arise on congenic (i.e., C57BL/6J and 129/SvImJ) backgrounds, which are particularly sensitive to the ablation of UCP1 (48) and thus may be prone to selection against enhanced ROS production, depending on breeding strategy. More generally, the functional effects that arise from distinct ROS sites in BAT on thermogenesis is an interesting avenue for future research.

The data presented herein indicate that mice genetically lacking UCP1 exhibit a plethora of acquired features that extend substantially beyond the deletion of UCP1 itself. These defects, such as the striking reduction of mitochondrial ETC components, should be considered when using this mouse model to study UCP1 function. Nonetheless, this model may have utility for examining the general features of mitochondrial dysfunction; for example, the molecular processes regulating the discordance between ETC protein and mRNA abundance in cold-exposed UCP1-KO animals may be an appropriate model for studying the fundamental mechanisms of mitochondrial proteostasis.

Materials and Methods

Animals. Mice were housed at 23 °C under a 12-h light/dark cycle with free access to food and water. All experiments used matched littermates. UCP1-KO mice and littermate UCP1-WT controls were generated by breeding heterozygous male and female (B6.129-Ucp1tm1Kz/J) mice as described previously (49). All animal experiments were performed in accordance with procedures approved by the Institutional Animal Care and Use Committee of the Beth Israel Deaconess Medical Center.

Mitochondrial Purification. BAT mitochondria were isolated as reported previously (17).

Measurement of Mitochondrial Ca^{2+} Uptake Capacity and Membrane Potential. The measurement of these parameters was performed simultaneously on a multichannel dye fluorimeter (C&L Instruments). The mitochondrial membrane potential ($\Delta\Psi$) was estimated by measuring changes in the fluorescence intensity of TMRM (60 nM; Molecular Probes) at excitation and emission wavelengths of 543 and 590 nm, respectively. Mitochondrial Ca^{2+} fluxes

were measured as changes in extramitochondrial [Ca^{2+}], which were followed by monitoring the fluorescence intensity of Calcium Green-5N (125 nM; Molecular Probes) at excitation and emission wavelengths of 482 and 535 nm, respectively. Mitochondria were challenged with single or multiple Ca^{2+} additions. Mitochondrial calcium retention capacity was determined as the amount of Ca^{2+} sequestered by mitochondria without incurring depolarization. Fluorimeter-based data were analyzed using Origin 8.0 (OriginLab).

Succinate + MitoQ. Mitochondria were added to buffer containing succinate (5 mM), followed by the addition of MitoQ (100 nM) and then GDP (1 mM). The mitochondria were challenged with calcium (15 μM) every 2 min until depolarization occurred.

Brown Fat Mitochondrial Calcium Uptake and Membrane Potential. Mitochondrial calcium uptake and membrane potential were monitored using a fluorescent spectrophotometer (C&L Instruments). Brown fat mitochondria were added to buffer (62.5 mM KCl, 5 mM Hepes pH 7.4, 0.1% BSA, 6 μM EDTA, 2 mM KH_2PO_4, 60 nM Calcium Green, and 1 μM TMRM). Mitochondria were respired off pyruvate and malate (5 mM each), succinate (5 mM) with or without rotenone (1 μM), or glycerol phosphate disodium salt hydrate (containing 50% β-isomer and 50% α-isomer) (5 mM) with or without rotenone. Next, GDP (1 mM) was added, and mitochondria were challenged with calcium (60 nmol calcium/mg mitochondrial protein) every 2 min until depolarization occurred.

Statistical Analysis. Data are presented as mean ± SEM. The unpaired two-tailed Student's *t* test and two-way ANOVA were used to determine statistical differences, with $P < 0.05$ considered to indicate statistical significance. Additional materials and methods can be found in *SI Materials and Methods*.

ACKNOWLEDGMENTS. We thank the members of the B.M.S. laboratory for helpful discussions. This work was supported by a Canadian Institutes of Health Research postdoctoral fellowship (to L.K.), a Human Frontier Science Program postdoctoral fellowship (to E.T.C.), the Wellcome Trust (Investigator Award 110159/Z/15/Z, to M.P.M.), the National Institutes of Health (Grants R01 DK102170 and R01 DK085171 to E.D.R., and R01 DK31405 to B.M.S.), and the JPB Foundation (B.M.S.).

1. Enerbäck S, et al. (1997) Mice lacking mitochondrial uncoupling protein are cold-sensitive but not obese. *Nature* 387:90–94.
2. Lidell ME, et al. (2013) Evidence for two types of brown adipose tissue in humans. *Nat Med* 19:631–634.
3. Jastroch M, Wuertz S, Kloas W, Klingenspor M (2005) Uncoupling protein 1 in fish uncovers an ancient evolutionary history of mammalian nonshivering thermogenesis. *Physiol Genomics* 22:150–156.
4. Oelkrug R, Goetze N, Meyer CW, Jastroch M (2014) Antioxidant properties of UCP1 are evolutionarily conserved in mammals and buffer mitochondrial reactive oxygen species. *Free Radic Biol Med* 77:210–216.
5. Clarke KJ, Porter RK (2013) Uncoupling protein 1 dependent reactive oxygen species production by thymus mitochondria. *Int J Biochem Cell Biol* 45:81–89.
6. Dlasková A, Clarke KJ, Porter RK (2010) The role of UCP 1 in production of reactive oxygen species by mitochondria isolated from brown adipose tissue. *Biochim Biophys Acta* 1797: 1470–1476.
7. Oelkrug R, Kutschke M, Meyer CW, Heldmaier G, Jastroch M (2010) Uncoupling protein 1 decreases superoxide production in brown adipose tissue mitochondria. *J Biol Chem* 285:21961–21968.
8. Shabalina IG, et al. (2014) ROS production in brown adipose tissue mitochondria: The question of UCP1-dependence. *Biochim Biophys Acta* 1837:2017–2030.
9. Stier A, et al. (2014) Mitochondrial uncoupling prevents cold-induced oxidative stress: A case study using UCP1 knockout mice. *J Exp Biol* 217:624–630.
10. Chouchani ET, et al. (2016) Mitochondrial ROS regulate thermogenic energy expenditure and sulfenylation of UCP1. *Nature* 532:112–116.
11. Chouchani ET, et al. (2014) Ischaemic accumulation of succinate controls reperfusion injury through mitochondrial ROS. *Nature* 515:431–435.
12. Murphy MP (2009) How mitochondria produce reactive oxygen species. *Biochem J* 417:1–13.
13. Scialò F, et al. (2016) Mitochondrial ROS produced via reverse electron transport extend animal lifespan. *Cell Metab* 23:725–734.
14. Cannon B, Nedergaard J (2004) Brown adipose tissue: Function and physiological significance. *Physiol Rev* 84:277–359.
15. Golozoubova V, Cannon B, Nedergaard J (2006) UCP1 is essential for adaptive adrenergic nonshivering thermogenesis. *Am J Physiol Endocrinol Metab* 291:E350–E357.
16. Matthias A, et al. (2000) Thermogenic responses in brown fat cells are fully UCP1-dependent: UCP2 or UCP3 do not substitute for UCP1 in adrenergically or fatty acid-induced thermogenesis. *J Biol Chem* 275:25073–25081.
17. Kazak L, et al. (2015) A creatine-driven substrate cycle enhances energy expenditure and thermogenesis in beige fat. *Cell* 163:643–655.
18. McAlister GC, et al. (2014) MultiNotch MS3 enables accurate, sensitive, and multiplexed detection of differential expression across cancer cell line proteomes. *Anal Chem* 86:7150–7158.
19. He J, et al. (2007) The AAA^+ protein ATAD3 has displacement loop binding properties and is involved in mitochondrial nucleoid organization. *J Cell Biol* 176:141–146.
20. Wang Y, Bogenhagen DF (2006) Human mitochondrial DNA nucleoids are linked to protein folding machinery and metabolic enzymes at the mitochondrial inner membrane. *J Biol Chem* 281:25791–25802.
21. West AP, et al. (2015) Mitochondrial DNA stress primes the antiviral innate immune response. *Nature* 520:553–557.
22. Kumari M, et al. (2016) IRF3 promotes adipose inflammation and insulin resistance and represses browning. *J Clin Invest* 126:2839–2854.
23. Kissig M, et al. (2017) PRDM16 represses the type I interferon response in adipocytes to promote mitochondrial and thermogenic programing. *EMBO J* 36:1528–1542.
24. Rongvaux A, et al. (2014) Apoptotic caspases prevent the induction of type I interferons by mitochondrial DNA. *Cell* 159:1563–1577.
25. Lemasters JJ, Theruvath TP, Zhong Z, Nieminen AL (2009) Mitochondrial calcium and the permeability transition in cell death. *Biochim Biophys Acta* 1787:1395–1401.
26. Luth ES, Stavrovskaya IG, Bartels T, Kristal BS, Selkoe DJ (2014) Soluble, prefibrillar α-synuclein oligomers promote complex I-dependent, $Ca2^+$-induced mitochondrial dysfunction. *J Biol Chem* 289:21490–21507.
27. Crompton M, Ellinger H, Costi A (1988) Inhibition by cyclosporin A of a $Ca2^+$-dependent pore in heart mitochondria activated by inorganic phosphate and oxidative stress. *Biochem J* 255:357–360.
28. Crichton PG, Parker N, Vidal-Puig AJ, Brand MD (2009) Not all mitochondrial carrier proteins support permeability transition pore formation: No involvement of uncoupling protein 1. *Biosci Rep* 30:187–192.
29. Hirst J, King MS, Pryde KR (2008) The production of reactive oxygen species by complex I. *Biochem Soc Trans* 36:976–980.
30. Quinlan CL, Perevoshchikova IV, Hey-Mogensen M, Orr AL, Brand MD (2013) Sites of reactive oxygen species generation by mitochondria oxidizing different substrates. *Redox Biol* 1:304–312.
31. De Meis L, Ketzer LA, Camacho-Pereira J, Galina A (2012) Brown adipose tissue mitochondria: Modulation by GDP and fatty acids depends on the respiratory substrates. *Biosci Rep* 32:53–59.
32. Chouchani ET, et al. (2016) A unifying mechanism for mitochondrial superoxide production during ischemia-reperfusion injury. *Cell Metab* 23:254–263.
33. Pryde KR, Hirst J (2011) Superoxide is produced by the reduced flavin in mitochondrial complex I: A single, unified mechanism that applies during both forward and reverse electron transfer. *J Biol Chem* 286:18056–18065.
34. Gyulkhandanyan AV, Pennefather PS (2004) Shift in the localization of sites of hydrogen peroxide production in brain mitochondria by mitochondrial stress. *J Neurochem* 90:405–421.
35. Hansford RG, Hogue BA, Mildaziene V (1997) Dependence of H_2O_2 formation by rat heart mitochondria on substrate availability and donor age. *J Bioenerg Biomembr* 29: 89–95.
36. Kushnareva Y, Murphy AN, Andreyev A (2002) Complex I-mediated reactive oxygen species generation: modulation by cytochrome c and $NAD(P)^+$ oxidation-reduction state. *Biochem J* 368:545–553.
37. Lambert AJ, Brand MD (2004) Inhibitors of the quinone-binding site allow rapid superoxide production from mitochondrial NADH:ubiquinone oxidoreductase (complex I). *J Biol Chem* 279:39414–39420.
38. Carraro M, Bernardi P (2016) Calcium and reactive oxygen species in regulation of the mitochondrial permeability transition and of programmed cell death in yeast. *Cell Calcium* 60:102–107.
39. Kelso GF, et al. (2001) Selective targeting of a redox-active ubiquinone to mitochondria within cells: Antioxidant and antiapoptotic properties. *J Biol Chem* 276: 4588–4596.
40. Kong X, et al. (2014) IRF4 is a key thermogenic transcriptional partner of PGC-1α. *Cell* 158:69–83.
41. Miwa S, St-Pierre J, Partridge L, Brand MD (2003) Superoxide and hydrogen peroxide production by *Drosophila* mitochondria. *Free Radic Biol Med* 35:938–948.
42. Mailloux RJ, Adjeitey CN, Xuan JY, Harper ME (2012) Crucial yet divergent roles of mitochondrial redox state in skeletal muscle vs. brown adipose tissue energetics. *FASEB J* 26:363–375.
43. Schönfeld P, Wojtczak L (2012) Brown adipose tissue mitochondria oxidizing fatty acids generate high levels of reactive oxygen species irrespective of the uncoupling protein-1 activity state. *Biochim Biophys Acta* 1817:410–418.
44. Shabalina IG, et al. (2006) UCP1 and defense against oxidative stress: 4-hydroxy-2-nonenal effects on brown fat mitochondria are uncoupling protein 1-independent. *J Biol Chem* 281:13882–13893.
45. Orr AL, Quinlan CL, Perevoshchikova IV, Brand MD (2012) A refined analysis of superoxide production by mitochondrial *sn*-glycerol 3-phosphate dehydrogenase. *J Biol Chem* 287:42921–42935.
46. Bernardi P, Di Lisa F (2015) The mitochondrial permeability transition pore: Molecular nature and role as a target in cardioprotection. *J Mol Cell Cardiol* 78:100–106.
47. Madungwe NB, Zilberstein NF, Feng Y, Bopassa JC (2016) Critical role of mitochondrial ROS is dependent on their site of production on the electron transport chain in ischemic heart. *Am J Cardiovasc Dis* 6:93–108.
48. Hofmann WE, Liu X, Bearden CM, Harper ME, Kozak LP (2001) Effects of genetic background on thermoregulation and fatty acid-induced uncoupling of mitochondria in UCP1-deficient mice. *J Biol Chem* 276:12460–12465.
49. Liu X, et al. (2003) Paradoxical resistance to diet-induced obesity in UCP1-deficient mice. *J Clin Invest* 111:399–407.
50. Elias JE, Gygi SP (2007) Target-decoy search strategy for increased confidence in large-scale protein identifications by mass spectrometry. *Nat Methods* 4:207–214.